Heliyon 9 (2023) e21781

Contents lists available at ScienceDirect

Heliyon

journal homepage: www.cell.com/heliyon

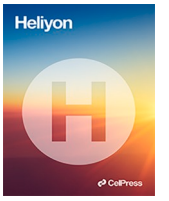

Synthesis of aromatic polynitroso compounds: Towards functional azodioxy-linked porous polymers

Nikola Cindro [1], Željka Car [1], Vesna Petrović Peroković [1], Mladen Borovina, Barbara Panić, Ivan Kodrin [*], Ivana Biljan [**]

Department of Chemistry, Faculty of Science, University of Zagreb, Horvatovac 102a, HR-10000 Zagreb, Croatia

A R T I C L E I N F O

Keywords:
Aromatic polynitroso compounds
Azodioxides
Cyclotrimerization
Polymer networks

A B S T R A C T

The polymerization property of aromatic polynitroso compounds could be used to create azodioxy porous networks with possible application for the adsorption of CO_2, the main greenhouse gas. Herein, we report the synthesis and characterization of new aromatic polynitroso compounds, with *para*-nitroso groups attached to the triphenylbenzene, triphenylpyridine, triphenyltriazine and triphenylamine moiety. The synthesis of the pyridine-based trinitroso compound was performed by reduction of the corresponding trinitro derivative to *N*-arylhydroxylamine followed by oxidation to the trinitroso product. For the synthesis of the benzene- and triazine-based trinitroso compounds, a novel synthetic strategy was implemented, which included cyclotrimerization of the 4-nitrosoacetophenone and 4-nitrosobenzonitrile, respectively. Reduction of the trinitro compound with triphenylamine unit produced the dinitroso product. In a solid state, all synthesized compounds form *E*-azodioxy oligomers or polymers. While azodioxy polymer with triphenylbenzene moiety is an amorphous solid, other azodioxy oligomers and polymers displayed sharp diffraction peaks pointing to their crystalline nature. A computational study indicated that eclipsed AA configurations are preferred over staggered AB and inclined AA' configurations. The serrated layers may be the most likely outcome when/if 2D layers form an organized polymer network of azodioxy linked triphenyltriazine-based building blocks.

1. Introduction

Aromatic C-nitroso compounds are well-known for their ability to dimerize or polymerize reversibly to *Z*- or *E*-azodioxides [1–9]. In a solid state, these compounds mostly appear as *E*-azodioxides while in solution nitroso monomer-azodioxide equilibrium is established which is usually shifted towards the *Z*-stereoisomers at low temperatures [1,3]. Under cryogenic conditions in solid state, azodioxy bond can be cleaved by UV light, and again regenerated by increase in temperature, rendering these systems as potential molecular OFF-ON switches [10–17]. Particularly interesting are compounds with multiple aromatic C-nitroso groups whose intermolecular interactions can lead to one-dimensional (1D), two-dimensional (2D) or three-dimensional (3D) polymeric azodioxides with various potential applications, *e.g.*, in organic electronics, gas storage and separation, and catalysis. Noteworthy, the polymerization of aromatic polynitroso compounds and the formation of azodioxy bonds occurs spontaneously at room temperature without the need for

* Corresponding author.
** Corresponding author.
E-mail addresses: ikodrin@chem.pmf.hr (I. Kodrin), ibiljan@chem.pmf.hr (I. Biljan).
[1] N.C., Ž.C. and V.P.P. contributed equally to this work.

https://doi.org/10.1016/j.heliyon.2023.e21781
Received 29 June 2023; Received in revised form 22 September 2023; Accepted 27 October 2023
Available online 7 November 2023

an initiator. The main representative of such compounds is 1,4-dinitrosobenzene (*para*-dinitrosobenzene) which forms 1D *E*-azodioxy polymer, poly(1,4-phenyleneazine-*N*,*N*-dioxide), of high thermal stability. Using the recently reported crystal structure of the 1,4-dinitrosobenzene polymer, its electronic properties were calculated, revealing that this 1D azodioxy polymer can be classified as a wide-bandgap organic semiconductor (OSC) with potential applications in photodetectors or light-emitting diodes (LEDs) [4,5]. This was further confirmed experimentally by diffuse reflectance spectroscopy measurements [5]. A series of aromatic dinitroso compounds were also recently evaluated as potential OSCs and several systems with interesting electronic properties were identified [5]. Mutual interactions of aromatic polynitroso compounds could be used to create 2D and 3D azodioxy-linked porous organic polymers (POPs). POPs are a class of porous materials constructed via strong covalent linkages between organic molecular building units [18,19]. Given the ongoing global concern related to elevated emissions of carbon dioxide (CO_2) into the atmosphere leading to global warming, climate change and rising sea levels [20,21], one of the most important potential applications of POPs is the capture of CO_2 [22–34]. POPs containing nitrogen-rich moieties, such as amine, imine, triazine, benzimidazole, carbazole, azo, etc., have recently emerged as promising materials for efficient and highly selective CO_2 capture and separation [22,35–41]. Among the mentioned functionalities, azo groups appear to be particularly effective in improving interactions between POPs and CO_2 and increasing CO_2/N_2 selectivity, even at elevated temperatures, making azo-linked POPs promising CO_2 adsorbents [42–48]. One of the drawbacks of azo-linked POPs is that they are usually obtained as amorphous materials due to the irreversible formation of azo bonds. Opposite of that, reversible formation of azodioxy bonds allows error corrections during polymerization and could lead to crystalline porous organic networks. Indeed, reversible self-addition polymerization of monomers with tetrahedrally oriented nitroso groups resulted with formation of large single crystals of diamondoid azodioxy networks [2]. Azodioxy linkages were also employed for preparation of crystalline porous materials by self-polymerization of tetrakis(arylnitroso)porphyrin [49]. These studies showed that aromatic derivatives with multiple nitroso groups can be used as building blocks for the design of new functional materials. However, due to the high reactivity of aromatic C-nitroso compounds, *e.g.*, the ease of their oxidation to nitro derivatives and the possibility of reaction with the starting material resulting in the formation of by-products, synthesis of these compounds is not straightforward and remains a challenge.

In our recent studies, we focused on the design and characterization of new POPs with various nitrogen-nitrogen linkages (azo, azoxy and azodioxy) and different trigonal connectors (triphenylbenzene, triphenylpyridine, triphenyltriazine and triphenylamine). We successfully synthesized new benzene-, pyridine- and triazine-based azo-bridged POPs and identified potential candidates for selective CO_2 adsorption [50,51]. In addition, we investigated computationally by using periodic DFT calculations and grand-canonical Monte Carlo (GCMC) simulations the effect of the abovementioned four trigonal connectors and three nitrogen-nitrogen linkages on the geometrical and adsorption properties of POPs [51,52]. The results obtained for computationally modeled porous organic systems suggested that the introduction of the azodioxy and azoxy linkages could lead to improved CO_2 adsorption capacity and higher CO_2 vs. N_2 selectivity when compared to azo linkages. These insights, along with the known reversibility in azodioxy bond formation which could result in crystalline porous organic networks, encouraged us to try to synthesize novel aromatic polynitroso compounds which could be used as starting building blocks for the creation of azodioxy networks. The targeted polynitroso compounds contain three *para*-nitrosophenyl rings, attached to the central benzene (**1**), pyridine (**2**), triazine (**3**) and amine (**4**) moiety (Fig. 1). Bearing in mind that the preparation of aromatic C-nitroso compounds is not simple, different synthetic methods were tested. The prepared compounds were characterized by FTIR spectroscopy, NMR spectroscopy, powder X-ray diffraction, elemental analysis, thermogravimetric analysis, N_2 adsorption-desorption experiments and computational methods.

2. Materials and methods

2.1. General information

All commercially obtained chemicals were used as received from suppliers. Thin-layer chromatography (TLC) was conducted with

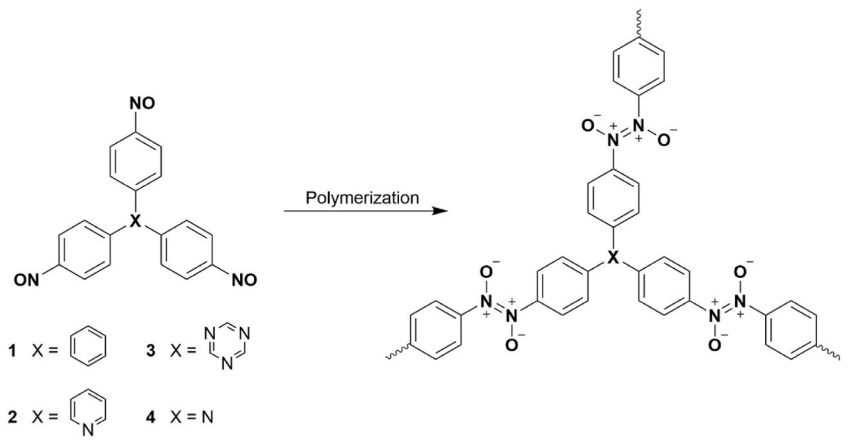

Fig. 1. Molecular structures of target aromatic polynitroso compounds and their possible polymerization to azodioxy networks.

silica gel 60-F254-coated plates (Merck). Column chromatography was performed using silica gel 60 (0.063−0.200 mm, Fluka). FTIR spectra were recorded on a PerkinElmer UATR Two spectrometer in the spectral range between 4000 cm^{-1} and 400 cm^{-1} at a resolution of 4 cm^{-1}, averaging 10 scans per spectrum. Solution-state NMR spectra were recorded on a Bruker Avance III HD 400 MHz at 25.0 °C. DMSO-d_6 or $CDCl_3$ were used as solvents and TMS as an internal standard for chemical shifts. Solid-state ^{13}C CP/MAS NMR spectra were recorded on a Bruker Avance Neo 400 MHz NMR spectrometer and Bruker Avance III HD 400 MHz NMR spectrometer at spinning rates of 12 and 15 kHz, respectively. Elemental analysis was provided by the Analytical Services Laboratory of the Ruđer Bošković Institute, Zagreb, Croatia. Thermogravimetric analysis was carried out using a simultaneous TGA-DTA analyzer Mettler-Toledo TGA/DSC 3+. Samples were placed in alumina pans (70 μL) and heated in flowing nitrogen (50 mL min^{-1}) from 30 °C up to 180 °C at a rate of 10 °C min^{-1} and held in isothermal conditions for 30 min at 180 °C to remove traces of solvents. Afterwards, samples were cooled to room temperature and heated in flowing nitrogen (50 mL min^{-1}) from 25 °C up to 800 °C at a rate of 10 °C min^{-1} and held in isothermal conditions for 15 min at 800 °C. To evaluate the thermal stability of the prepared compounds samples (of up to ~ 5 mg) were heated in flowing nitrogen (50 mL min^{-1}) from 30 °C to 180 °C and held at isothermal conditions for 10 min. IR spectra were recorded immediately upon cooling of the samples and compared with IR spectra of starting compounds. CO_2 sorption experiments were carried out by following a previously reported procedure with minor modifications in experimental conditions [53]. Before performing CO_2 adsorption experiments, a fresh sample (~17−20 mg) was placed in a 70 μL alumina pan, heated to 100 °C at a heating rate of 20 °C min^{-1} in nitrogen atmosphere (flow rate 150 mL min^{-1}) and held at 100 °C for 30 min to dry the sample. After drying, CO_2 adsorption was measured by switching between N_2 atmosphere and CO_2 atmosphere in 20 min intervals (flow rates for both gases were 150 mL min^{-1}) at ~30 °C. The measured sample temperature varied around 33 °C during the whole experiment. To correct for different buoyancy effects on the TG scale and alumina pan, a baseline curve was recorded under the same experimental conditions using an empty alumina pan and subtracted from the measured curve. Data collection and analysis were performed using the program package STARe Software 16.40 MettlerToledo GmbH. PXRD diffractograms were recorded on a Malvern Panalytical Aeris powder diffractometer in the Bragg-Brentano geometry with PIXcel1D detector. The specific surface area was determined from nitrogen (N_2) gas adsorption-desorption data obtained with Micromeritics ASAP-2000 at 77 K. Prior to analysis, samples were degassed at 150 °C under a dynamic vacuum of 7 mPa. The adsorption data were used to calculate the surface area with the Brunauer–Emmett–Teller (BET) model, while the pore size distribution was determined with the Barrett-Joyner-Halenda (BJH) method.

2.2. Synthesis

2.2.1. Synthesis of 1,3,5-tris(4-nitrosophenyl)benzene (1)

In a 50 mL round bottom flask 4-nitrosoacetophenone (500 mg, 3.4 mmol) was suspended in 20 mL of absolute ethanol. The mixture was stirred and heated to reflux turning suspension into green solution. At this point, 1.0 mL of thionyl chloride was carefully added and mixture was heated under reflux for 5 h. Clear green solution turned into brown suspension and product started to precipitate. After cooling to room temperature suspension was stirred for further 16 h and filtered, yielding 250 mg of brown precipitate. The precipitate was washed with DCM, acetone, DMSO and finally DCM again yielding 140 mg (28 %) of compound **1**.

Elemental Analysis: 66.93 %C (calc. 70.84), 4.13 %H (calc. 4.09), 9.60 %N (calc. 10.33).

2.2.2. Synthesis of 2,4,6-tris(4-nitrosophenyl)pyridine (2)

In a 100 mL round bottom flask 2,4,6-tris(4-nitrophenyl)pyridine (1.99 g, 4.5 mmol) was suspended in acetone (34 mL) and THF (14 mL). Ammonium chloride (0.99 g, 18.5 mmol) and activated zinc powder (2.5 g, 38.2 mmol) were added next and the suspension was stirred at room temperature for 3.5 h. Reaction mixture was filtered and the filtrate cooled to 0 °C in an ice bath. Cold aqueous solution of iron(III) chloride hexahydrate (75 mL, 0.02 g/mL) was added next and the mixture was stirred at 0 °C for 5 min. It was extracted with ethyl acetate and the organic layer was evaporated *in vacuo* until 5−10 mL of the organic solvent remained in the flask. 20 mL of methanol was added to the mixture next, and flask was sealed and left at room temperature for 7 days. The beige precipitate was filtered, washed with acetone excessively and dried yielding 164 mg (9 %) of compound **2**.

Elemental Analysis: 62.82 %C (calc. 70.05), 3.81 %H (calc. 3.58), 12.17 %N (calc. 14.21).

2.2.3. Synthesis of 2,4,6-tris(4-nitrosophenyl)-1,3,5-triazine (3)

4-Nitrosobenzonitrile (150 mg, 1.14 mmol) was taken in a round bottom flask. Then 0.35 mL (4 mmol) trifluoromethanesulfonic acid was added dropwise for 10 min at 0 °C. The reaction mixture was stirred for 18 h at 110 °C in an argon atmosphere. After that, 3 mL of water was added to the reaction mixture and dark brown product started to precipitate. The precipitate was filtered and washed several times with water, acetone and DCM yielding 129 mg (85 %) of compound **3**.

Elemental Analysis: 43.87 %C (calc. 63.64), 3.09 %H (calc. 3.05), 14.10 %N (calc. 21.20).

2.3. Computational details

The final geometries for simulation of PXRD patterns were taken from our previous papers [51,52]. To complete the triphenylbenzene and tryphenyltriazine series four new geometries ($\mathbf{1}_{\mathbf{incl}}$, $\mathbf{1}_{\mathbf{serr}}$, $\mathbf{3}_{\mathbf{incl}}$ and $\mathbf{3}_{\mathbf{serr}}$) were generated and optimized. Periodic density functional theory (DFT) calculations were performed in CRYSTAL17 [54]. We used PBE functional with Grimme's D3 correction for a better description of the weak dispersive interactions [55,56]. Triple-zeta basis set pob-TZVP-rev2 was used on all atoms [57]. The input files for CRYSTAL17 were created from cif files with cif2cell package [58]. Full optimizations were performed with default convergence criteria. Total energy convergence was set to 10^{-7} and truncation criteria for the calculations of Coulombs

and exchange integrals increased to (8 8 8 8 16) for SCF calculations. The reciprocal space was sampled with appropriate Pack-Monkhorst k-point mesh (usually 2 × 2 x 8). The lattice parameters of the DFT-optimized structures are given in Table S2 (Supporting Information). The results were visualized in VESTA [59]. The optimized geometries were finally saved as cif files, and PXRD simulated in Mercury [60]. The reported CO_2 uptakes at 298 K and 1 bar were taken from our previous papers where we have described GCMC procedures [51,52].

3. Results and discussion

3.1. Synthesis and characterization

Aromatic C-nitroso compounds appear as intermediates on the redox scale between nitroarenes and anilines. The classic methods for their preparation involve (i) partial reduction of the aromatic nitro derivative to *N*-arylhydroxylamine followed by oxidation to nitrosobenzene, and (ii) direct oxidation of anilines to the corresponding aromatic C-nitroso compounds [3,61]. The main problems associated with these approaches include finding the proper conditions to prevent over-reduction and over-oxidation of the desired nitroso product, and to avoid or diminish formation of side products, such as azo and azoxy compounds. An attempt to prepare the trinitroso compound **1** by reduction of the 1,3,5-tris(4-nitrophenyl)benzene (TNPB) to the corresponding *N*-arylhydroxylamine and its subsequent *in situ* oxidation was unsuccessful due to the very low solubility of the starting TNPB in the solvents used for the reaction. We also tried an oxidation reaction of 1,3,5-tris(4-aminophenyl)benzene (TAPB) with Oxone® but this led to a complex mixture of products which could not be separated and characterized. Therefore, we tested a new synthetic strategy towards trinitroso compound **1** which included cyclotrimerization reaction of 4-nitrosoacetophenone mediated by thionyl chloride in absolute ethanol (Fig. 2a). Starting 4-nitrosoacetophenone was prepared by oxidation of 4-aminoacetophenone by Oxone® (Supporting Information). The FTIR spectrum of the cyclotrimerization product **1** revealed the presence of a band at 1262 cm^{-1}, assigned to the asymmetric stretching vibration of the *E*-azodioxy group (Fig. 2b). The position of this and other bands differs from those present in the IR spectrum of the starting 4-nitrosoacetophenone (Fig. S4), indicating formation of new product.

Furthermore, the bands characteristic for nitroso monomers do not appear in the FTIR spectrum of the product, suggesting there are no observable amount of the nitroso end-groups. Additionally, we could observe a band at 1686 cm^{-1} which could be attributed to the stretching vibration of the carbonyl group. However, the intensity of this band is relatively low when compared to *e.g.,* carbonyl stretching vibration band at 1683 cm^{-1} in the spectrum of the starting 4-nitrosoacetophenone (Fig. S4), indicating that it probably corresponds to residual carbonyl groups present in the final material. Noteworthy, this band could be detected in the spectrum of the product even after extensive washing of the sample with various organic solvents such as DCM, acetone and even hot DMSO. Since the

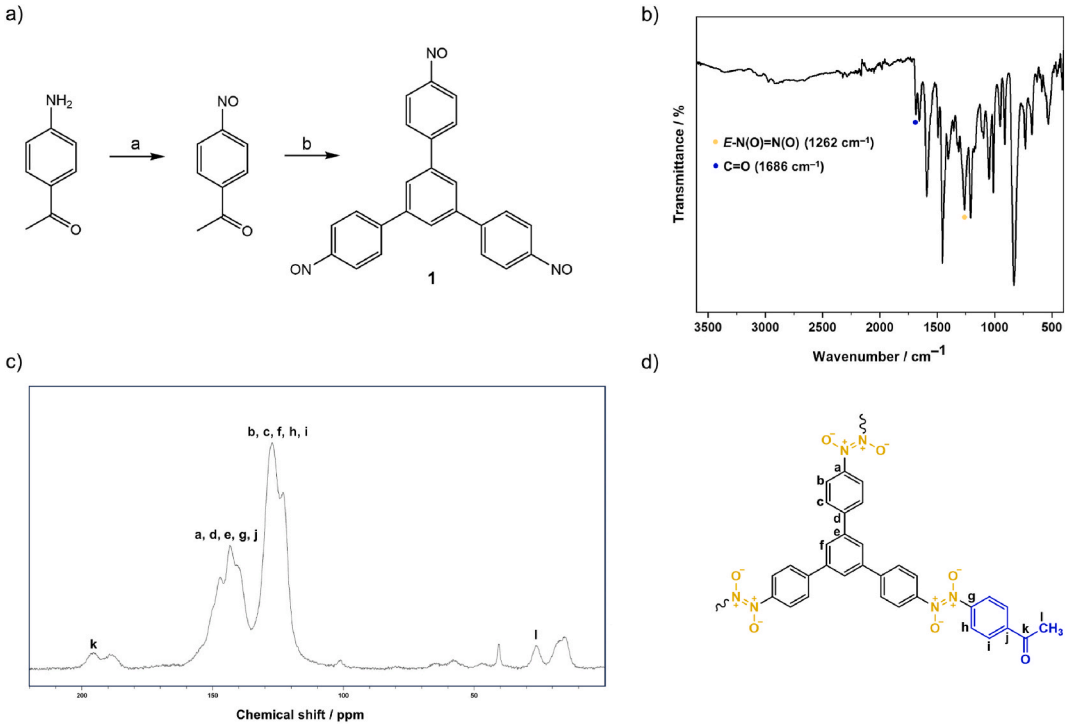

Fig. 2. a) Synthesis route to 1,3,5-tris(4-nitrosophenyl)benzene (**1**). Reaction a: Oxone®, H_2O, DCM, rt, 20 min, 43 %. Reaction b: $SOCl_2$, abs. EtOH, 5 h, reflux, 28 %. b) FTIR spectrum of azodioxy polymer of **1**. c) ^{13}C CP/MAS NMR spectrum of azodioxy polymer of **1**. d) Proposed molecular structure of azodioxy polymer of **1**.

isolated product is insoluble in common organic solvents, we acquired its ^{13}C CP/MAS solid-state NMR spectrum (Fig. 2c). Inspection of the ^{13}C CP/MAS NMR spectrum showed the aromatic carbon signals located in the range $\delta = 123-147$ ppm. The signal at 143 ppm probably belongs to the carbon attached to the *E*-azodioxy group (marked with a in Fig. 2c), while there is no signal of the carbon bonded to the monomeric nitroso group (−C–N═O) usually situated around 165 ppm [62], which agrees with the FTIR results. In addition, the ^{13}C CP/MAS spectrum also indicated the presence of the carbonyl group at 196 ppm (marked with k in Fig. 2c) and in the aliphatic region of the spectrum we could observe the signal of methyl group at 26.6 ppm (marked with l in Fig. 2c). The collected data suggested that in the final material the triphenylbenzene building units are connected through *E*-azodioxy bonds with acetophenone moieties situated at the end of the polymer (Fig. 2d). These acetophenone terminal moieties could be attached to the polymer backbone by intermolecular formation of *E*-azodioxy bonds between nitroso groups of **1** and those of 4-nitrosoacetophenone, which is present in the reaction mixture (Fig. S1). Previously, we found that formation of such cross-linked azodioxides is possible both in solution and in solid state [63,64].

The synthesis of the pyridine-based trinitroso compound **2** was carried out by the reduction of the 2,4,6-tris(4-nitrophenyl)pyridine (TNPP) to the corresponding *N*-hydroxylamine, followed by its *in situ* oxidation (Fig. 3a). The starting TNPP was prepared by the microwave-assisted synthesis via a modified Chichibabin reaction, optimized herein (Supporting Information), in 30 min with a yield of 59 %. This is faster than the usual synthesis, which takes 3 h with a comparable yield of 58 % according to literature procedure [65], or 3.5 h and a yield of 50 % by following the procedure described in this work (Supporting Information). The reaction was optimized with respect to reaction time, temperature and the amount of ammonium acetate and acetic acid added (Table S1). Optimal yields were achieved with the amount of ammonium acetate (13 equiv.) comparable to the classic synthesis [65] but it was found that the reaction can be performed with less acetic acid (16 equiv., entry 6, Table S1 in comparison to 44 equiv. in classic conditions). The main product in entries 1−3 (Table S1) was one of the precursors in modified Chichibabin reaction, compound A (Fig. S3) which indicates how important the addition of ammonium acetate and acetic acid is for the reaction completion. The solubility of the main product (TNPP) is rather low in standard organic solvents, therefore its ^{1}H NMR spectrum was recorded in hot DMSO-d_6 (Fig. S2). The ^{1}H NMR spectrum of TNPP obtained under microwave conditions was comparable to the spectrum of the compound prepared in classic route. Reduction of TNPP with zinc and ammonium chloride followed by oxidation step with iron(III) chloride hexahydrate resulted in a solid product of poor solubility in common organic solvents. Comparison of the FTIR spectra of the obtained product (Fig. 3b) and starting TNPP (Fig. S5) indicated complete disappearance of signals assigned to asymmetric and symmetric N–O stretching vibrations of nitro group confirming the formation of new product. The FTIR spectrum of the product revealed the presence of a new intense band at 1506 cm^{-1}, attributed to nitroso monomer N═O stretching vibration, along with a band at 1250 cm^{-1} characteristic for the *E*-azodioxy group (Fig. 3b). FTIR data were corroborated with the ^{13}C CP/MAS NMR spectrum of the product (Fig. 3c) which showed signals at 118.5, 128.6, 143.6, 152.9 and 165.2 ppm, assigned to the aromatic carbons in phenyl and pyridine rings. Noteworthy, chemical shift at 165.2 ppm (marked with l in Fig. 3c) is assigned to the carbon directly bonded to the nitroso group (−C–N═O). The signal at 143.6

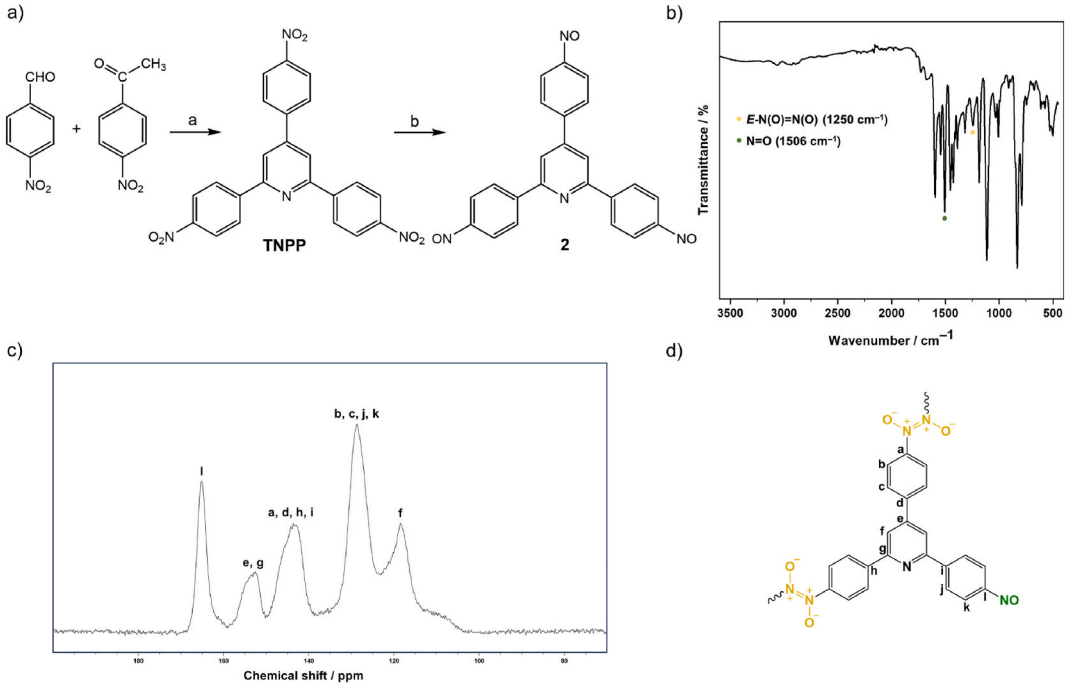

Fig. 3. a) Synthetic route to 2,4,6-tris(4-nitrosophenyl)pyridine (**2**). Reaction a: NH_4OAc, AcOH, reflux, 3.5 h, 50 %. Reaction b: (i) Zn, NH_4Cl, THF, acetone, rt, 3.5 h; (ii) $FeCl_3 \times 6H_2O$, 0 °C, 5 min, 9 %. b) FTIR spectrum of azodioxy oligomer of **2**. c) ^{13}C CP/MAS NMR spectrum of azodioxy oligomer of **2**. d) Proposed molecular structure of azodioxy oligomer of **2**.

ppm (marked with a in Fig. 3c) probably belongs to the carbon attached to the *E*-azodioxy group, however, it overlaps with the chemical shifts of other quaternary carbons. The above-mentioned data suggested formation of *E*-azodioxy oligomers of **2** with unreacted nitroso end-groups (Fig. 3d).

As in the case of trinitroso derivatives **1** and **2**, the first attempt to synthesize triazine-based trinitroso derivative **3** included the reduction of the 2,4,6-tris(4-nitrophenyl)-1,3,5-triazine (TNPT) with zinc and ammonium chloride to the *N*-hydroxylamine followed by oxidation step with iron(III) chloride. Unfortunately, this reaction proceeded with very poor yield and low reproducibility, preventing a detailed structural characterization of the obtained product. Therefore, we tested other possible synthetic approaches towards the trinitroso derivative **3**. Among them, we first tried the oxidation reaction of 1,3,5-tris-(4-aminophenyl)triazine (TAPT) with Oxone®. However, this approach was unsuccessful, similarly to the case of derivative **1**, resulting in the formation of a complex mixture of products, none of which could be identified as the desired trinitroso compound **3**. Next, we tried a novel synthetic strategy, which included cyclotrimerization of 4-nitrosobenzonitrile (Fig. 4a), prepared by oxidation of 4-aminobenzonitrile with Oxone® (Supporting Information). By adapting a slightly modified strategy for the synthesis of TNPT and TAPT by superacid-catalyzed cyclotrimerization of 4-nitrobenzonitrile and 4-aminobenzonitrile, respectively [66,67], we obtained a solid product, insoluble in common organic solvents, in a very good yield (85 %). Comparison of the FTIR spectra of the isolated product (Fig. 4b) and starting 4-nitrosobenzonitrile (Fig. S6) revealed disappearance of the C ≡N stretching band at 2238 cm^{-1} in the spectrum of the product suggesting the completion of the trimerization reaction. The observation of bands at 1616 and 1388 cm^{-1} further indicated the formation of triazine rings [68,69]. FTIR spectrum of the product also revealed the presence of a strong band at 1244 cm^{-1} assigned to asymmetrical stretching vibration of the *E*-azodioxy bond. The successful formation of *E*-azodioxy polymer of **3** was corroborated by inspection of ^{13}C CP/MAS NMR spectrum which showed signals at 167.4, 143.6, 132.6 and 119.3 ppm (Fig. 4c). The signal at 167.4 ppm is attributed to triazine carbon atom (marked with e in Fig. 4c) [70], whereas the signal at 143.6 ppm is assigned to the carbon bonded to the *E*-azodioxy group (marked with a in Fig. 4c). The signals at 132.6 and 119.3 ppm originate from phenyl carbons in different chemical environments. The absence of signal at 165 ppm, characteristic for the –C–N═O moiety, confirmed formation of polymer network of **3** with *E*-azodioxy linkages (Fig. 4d).

In order to synthesize trinitroso derivative **4** containing amine central moiety, commercially available tris(4-nitrophenyl)amine (TNPA) was reduced in the presence of zinc and ammonium chloride to the intermediate *N*-hydroxylamine derivative which was in the next step oxidized by iron(III) chloride (Supporting Information). The obtained solid was poorly soluble in DMSO and practically insoluble in other common organic solvents. The ^{1}H NMR spectrum of the product recorded in DMSO-d_6 (Fig. S8) revealed four new sets of signals, in addition to the impurity signals belonging to the starting TNPA. Analysis of the ^{1}H NMR spectrum indicated that the product is not the trinitroso derivative **4**, for which we would expect only two pairs of signals, but a dinitroso derivative **4a**, with the third group on the phenyl ring probably being nitro. This was further supported by inspection of FTIR spectra of the product which

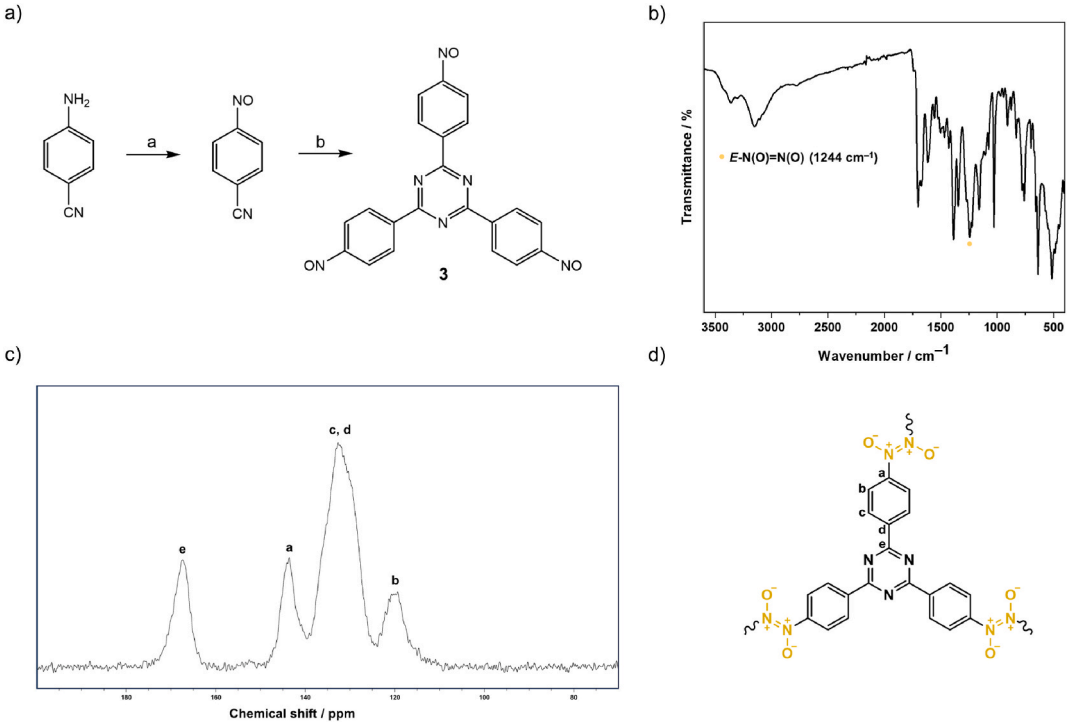

Fig. 4. a) Synthesis route to 2,4,6-tris(4-nitrosophenyl)-1,3,5-triazine (**3**). Reaction a: Oxone®, H_2O, DCM, rt, 20 min, 51 %. Reaction b: CF_3SO_3H, 10 min, rt, 18 h, 110 °C, Ar, 85 %. b) FTIR spectrum of azodioxy polymer of **3**. c) ^{13}C CP/MAS NMR spectrum of azodioxy polymer of **3**. d) Proposed molecular structure of azodioxy polymer of **3**.

revealed an intense band at 1268 cm^{-1}, attributed to asymmetrical stretching vibration of the *E*-azodioxy bond, and bands corresponding to stretching vibrations of nitro group at 1339 cm^{-1} and monomeric nitroso end-groups at 1491 cm^{-1} (Fig. S7). To further characterize the solid-state structure of the obtained product, we acquired its ^{13}C CP/MAS NMR spectrum (Fig. 5) which showed characteristic signals of carbon atoms attached to the nitroso group ($\delta = 163.6$ ppm, marked with a in Fig. 5), *E*-azodioxy and nitro groups ($\delta = 142.3$ ppm, marked with h and l, respectively, in Fig. 5) together with the chemical shifts of the other aromatic carbons at 123.1, 126.1, 145.2 and 150.3 ppm. These results indicated that in the solid state dinitroso derivative **4a** forms *E*-azodioxy oligomers with free nitroso end-groups (Fig. 5). Since the reduction method did not result with the desired trinitroso derivative **4**, we examined another frequently used synthetic approach towards the aromatic C-nitroso compounds which includes oxidation of corresponding amino derivatives. Unfortunately, the oxidation of the triamino derivative tris(4-aminophenyl)amine (TAPA) with Oxone® produced a complex reaction mixture without an observable amount of compound **4**. Another approach that was tried relied on nitrosation using $NOBF_4$. Starting triphenylamine was brominated using NBS and the resulting tris(4-bromophenyl)amine was further treated with *n*-BuLi followed by TMSCl to produce tris(4-trimethylsilylphenyl)amine. The TMS amine was then treated under various conditions (including mechanochemical) with $NOBF_4$ to produce compound **4**. Unfortunately, none of the conditions tried led to the formation of the trinitroso derivative **4.**

Thermal stability of isolated azodioxy oligomers/polymers of **1**, **2**, **3** and **4a** was investigated using TGA by heating the samples up to 800 °C at a heating rate of 10 °C min^{-1} in N_2 atmosphere. To remove traces of solvents or adsorbed water, all samples were heated to 180 °C at a heating rate of 10 °C min^{-1} in N_2 atmosphere and held at isothermal conditions for 30 min. Compounds **1**, **2** and **4a** showed minimal weight loss (<0.1 mg) during the drying process and remained stable during the isothermal step at 180 °C (Figures S9, S10 and S12). In comparison, compound **3** immediately started to lose mass and up to 80 °C had lost around 20 % of its initial weight (~1.8 mg per 9.3 mg), while its remaining mass remained stable up to 180 °C and during the isothermal step (Fig. S11). All samples were visually examined after drying and showed no noticeable discoloration or other visible changes, while after heating to 800 °C they changed color to a grayish black and there was a noticeable change in volume. Additionally, subsequent experiments were carried out to confirm the stability of the studied compounds and IR spectra were recorded after the sample was heated to 180 °C in flowing nitrogen and held at isothermal conditions for 10 min. IR spectra of compounds heated to 180 °C showed no significant differences compared to the spectra of unheated compounds which indicates that no notable changes occurred to the material at those conditions (Fig. S23). TGA traces (Fig. S9–S12) showed that the obtained products exhibit good thermal stability. They are stable up to around 220 °C at which point they begin to lose mass. Compounds **1** and **2** displayed a gradual loss of mass over the entire temperature range and eventually lost about 1/3 of the initial mass at temperatures around 700 °C or higher. Compound **3** also began to decompose at around 220 °C but its decomposition process was much more rapid and it lost 1/3 of the initial mass up to temperatures around 400 °C at which point the decomposition rate decreased and the sample gradually lost a further 20 % of its initial mass up to temperatures of 800 °C. Compound **4a** displayed similar behavior as compounds **1** and **2** with a gradual decrease in mass up until 340 °C, after which the decomposition rate increased up to temperatures around 450 °C when it decreased again and remained constant during the rest of the experiment.

The results of the elemental analysis revealed some deviations from the calculated values, especially for polymer of **3**. This can be attributed to adsorption of moisture and incomplete polymerization and is frequently observed in porous organic polymers [44,45].

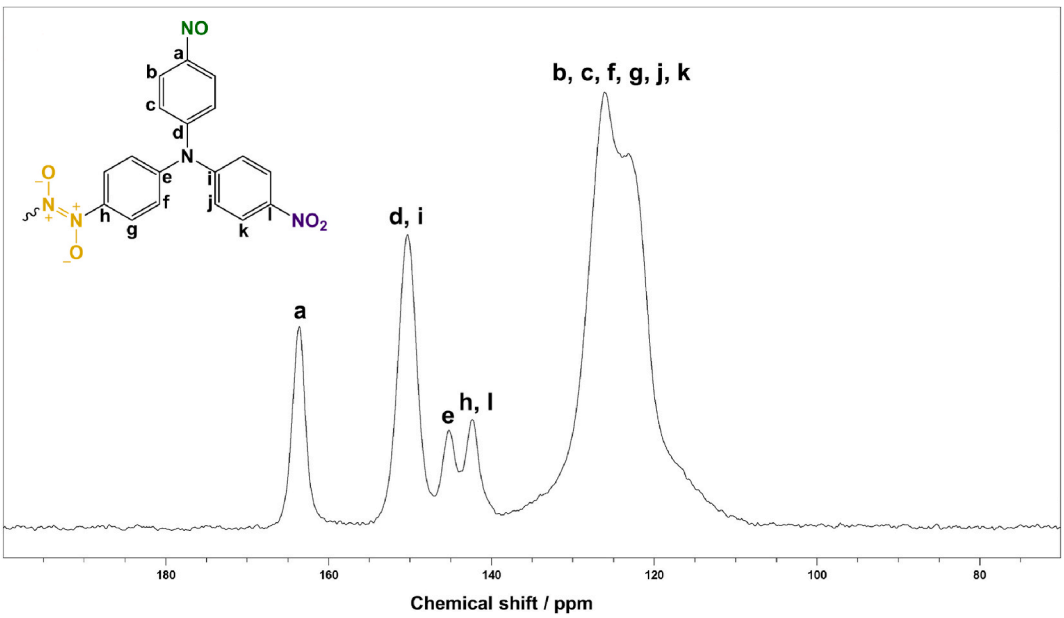

Fig. 5. ^{13}C CP/MAS NMR spectrum and the proposed molecular structure of azodioxy oligomer of **4a**.

3.2. Comparison of experimental and computational data

As indicated in the Introduction section, polymerization of aromatic polynitroso derivatives could lead to the formation of crystalline porous networks. To evaluate crystallinity of the obtained azodioxy oligomers/polymers of **1**, **2**, **3** and **4a**, we performed PXRD experiments. Unlike the PXRD pattern of azodioxy polymer of **1** which showed broad diffraction peak, indicating its amorphous nature without long-range order, the PXRD patterns of azodioxy oligomers/polymers of **2**, **3** and **4a** revealed sharp peaks suggesting that they are crystalline materials (Fig. 6, Fig. S14−S17). To correlate the experimentally obtained PXRD patterns with 3D periodic structures of targeted compounds, first we optimized four different configurations, which mostly differ in a relative arrangement of the neighboring 2D layers, in which trigonal building units are connected by *E*-azodioxy bonds. Depending on the slipping direction, the eclipsed AA configuration can be transformed either into inclined AA' or serrated AA' and further into AB configurations, as demonstrated on triphenyltriazine derivative **3** (Fig. 7), for which we experimentally confirmed formation of polymer network through *E*-azodioxy linkages. To complete the series of different stacking modes reported in our previous papers [51,52], we have conducted additional periodic DFT calculations and simulated PXRD patterns based on their optimized geometries (Table S2, Fig. 6, S13–S17) for all four target compounds. Based on the literature data for other covalent organic frameworks that show high crystallinity, *e.g.* imine linked polymers constituted of the same trigonal connectors [71–73], eclipsed AA configuration was also expected to be the most stable in herein investigated configurations. While eclipsed AA dominates in hypothetical triphenylbenzene ($\mathbf{1_{AA}}$), introduction of nitrogen-rich moieties in trigonal connectors triggers a possibility of different stacking modes to appear, especially for triphenyltriazine system, where the energy difference between the $\mathbf{3_{serr}}$ and $\mathbf{3_{AA}}$ becomes very small (Table S2). The experimental PXRD of **3** shows two dominant peaks around at $2\theta = 14.8°$ and 27.0°. While there is no significant difference between PXRD patterns of $\mathbf{3_{serr}}$ and $\mathbf{3_{AA}}$ in the low-angle region, the experimental PXRD pattern and the simulated one for $\mathbf{3_{serr}}$ almost perfectly match for the peak at $2\theta = 27.0°$, suggesting that 2D layers are slightly displaced (Fig. 6, grey line).

This also corroborates other structural studies on similar systems, suggesting that slipped configurations are also energetically favorable and that eclipsed structures can be an oversimplification of the true local environment [74–76]. Although the overlap between the experimental and simulated PXRD patterns of triphenylamine-based derivative also suggests slipping of the neighboring layers, a straightforward correlation is not possible because spectroscopic characterization confirmed the formation of dinitroso derivative **4a** which appears as *E*-azodioxy oligomer with free nitroso end-groups in solid state, and not the polymer network as in **3**.

The porosity of azodioxy oligomers/polymers of **1**, **2**, **3** and **4a** was investigated by using N_2 adsorption-desorption isotherms at 77 K (Fig. 8a and S18). All samples were degassed at 150 °C under vacuum prior to the analysis. The specific surface areas were calculated by using the BET model and were 2.4, 48.1, 4.4 and 14.0 $m^2\ g^{-1}$ for oligomers/polymers of **1**, **2**, **3** and **4a**, respectively (Table 1). According to the pore size distribution (Fig. S18), all four materials exhibit a mesoporous nature with a proportion of pores greater than 50 nm, the latter being especially pronounced for polymer of **1**. Oligomers/polymers of **2**, **3** and **4a** also possess a small amount of micropores.

A high value of BET surface area is not necessarily a deciding factor for the CO_2 capture capacity, and materials with moderate porosities and BET surface areas lower than 100 $m^2\ g^{-1}$ can display enhanced CO_2 gas sorption properties [22,42,77]. Therefore, we investigated CO_2 adsorption of azodioxy oligomers/polymers of **1**, **2**, **3** and **4a** by using thermogravimetric analysis and the obtained data are summarized in Table 1. Compounds **1** and **2** show relatively sharp adsorption profiles where the sample mass readily increases upon switching to CO_2 atmosphere and readily decreases when returning to N_2 atmosphere (Figs. S19 and 8b). Compounds **3** and **4a** exhibit a more complex response, where the CO_2 uptake is more gradual and reaches equilibrium levels after 10 min, but the mass decrease upon switching back to N_2 atmosphere is gradual as well (Figs. S21 and S22). While most of the mass loss for compound **4a** occurs within 5 min of switching back to N_2 the mass still remains higher than it was at the beginning of the experiment and gradually decreases during the whole 20-min interval. Even more interesting is the behavior of compound **3,** where the mass decrease upon switching back to N_2 atmosphere is far less pronounced and the sample retains a significantly higher mass throughout the whole 20-min interval in N_2 atmosphere. This would suggest that compounds **3** and **4a** show a higher preference for CO_2 than for N_2, which is

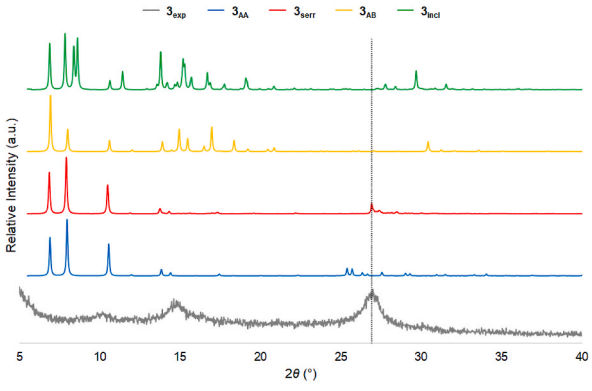

Fig. 6. Experimental and the simulated PXRD patterns of azodioxy polymer of **3** (eclipsed AA, serrated AA', staggered AB and inclined AA'). The grey dotted line shows a peak at $2\theta = 27.0°$.

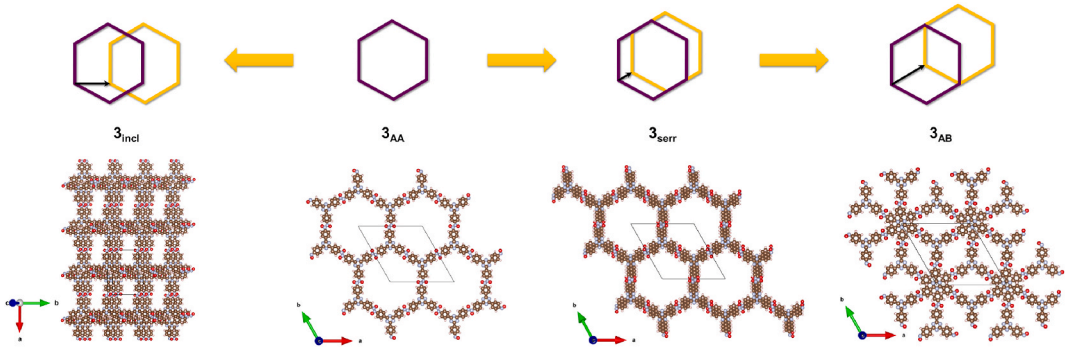

Fig. 7. Four different 2D layer-stacking modes of azodioxy polymer of **3** (inclined AA', eclipsed AA, serrated AA' and staggered AB).

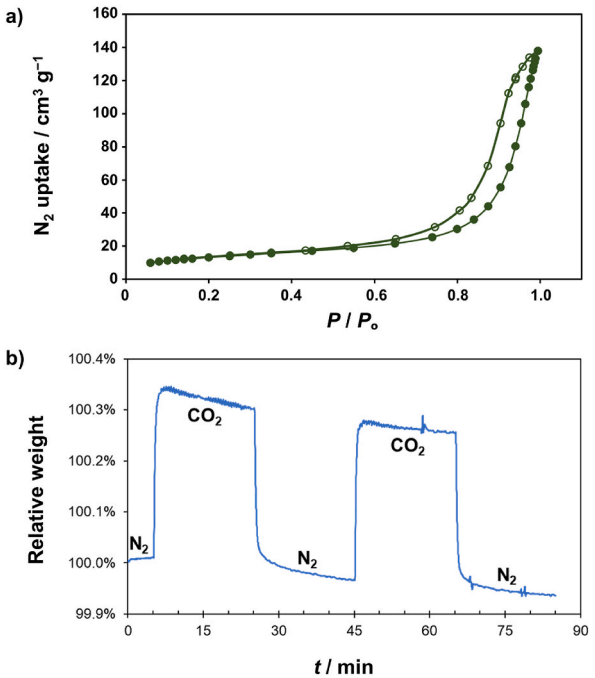

Fig. 8. a) N_2 adsorption-desorption isotherms of azodioxy oligomer of **2** measured at 77 K. The adsorption and desorption isotherms are depicted with filled and open markers, respectively. b) Thermogravimetric CO_2 adsorption and desorption profile at approximately 303 K and 150 mL min^{-1} CO_2 and N_2 flow rates for azodioxy oligomer of **2**.

Table 1
BET surface areas (S_{BET}) and CO_2 uptakes (experimental and simulated) of azodioxy oligomers/polymers of **1**, **2**, **3** and **4a**.

Compound	S_{BET} (m^2 g^{-1})	CO_2 uptake (mg g^{-1}) experimental	CO_2 uptake (mg g^{-1}) simulated for AA configuration[a]
1	2.4	4.2	30.5
2	48.1	3.2	24.5
3	4.4	6.0	21.1
4a	14.0	6.2	48.3[b]

[a] Calculated CO_2 uptakes for eclipsed AA configurations from GCMC simulations at 1 bar and 298 K reported in our previous papers [51,52].
[b] Calculated CO_2 uptake for the azodioxy polymer of the target trinitroso derivative **4**.

especially pronounced for compound **3**.

Our previous computational studies suggested that azodioxy linkages show a higher potential for the adsorption of CO_2 in comparison with other nitrogen-nitrogen linkages [51,52]. Although it is quite difficult to directly compare the GCMC calculated CO_2 adsorption data (at 298 K and 1 bar) with the experimental results (at approximately 303 K) without a full confirmation that highly arranged polymer networks are formed during polymerization, CO_2 uptakes calculated for the hypothetical eclipsed AA configurations

suggest that azodioxy-linked triphenylamine $\mathbf{4_{AA}}$ shows the highest affinity toward CO_2 binding among the all investigated compounds in eclipsed AA configuration (48.3 mg g^{-1}). The experimental results also showed the highest adsorption of CO_2 (6.2 mg g^{-1}) for the azodioxy oligomer derived from dinitroso derivative **4a**. Any further slipping of layers will increase CO_2 uptake according to our previous computational studies [51,52]. However, it should be mentioned that CO_2 adsorption capacity highly depends on various factors, not only on the 2D layer stacking modes.

4. Conclusions

Using different synthetic approaches, we prepared four new aromatic polynitroso compounds, containing *para*-nitroso functionalities attached to triphenylbenzene, triphenylpyridine, triphenyltriazine and triphenylamine unit and investigated their potential as building blocks for azodioxy polymer networks. For the synthesis of benzene- and triazine-based trinitroso derivatives, novel synthetic strategy was employed which included cyclotrimerization of the 4-nitrosoacetophenone and 4-nitrosobenzonitrile, respectively. Pyridine-based trinitroso and amine-based dinitroso compounds were synthesized by classic method which involved partial reduction of the corresponding nitro derivatives to *N*-arylhydroxylamines followed by oxidation to nitroso derivatives. The obtained trinitroso derivatives with triphenylbenzene and triphenyltriazine moieties self-polymerized to *E*-azodioxy linked polymers, whereas pyridine-based trinitroso and amine-based dinitroso compounds formed *E*-oligomers in solid state, with unreacted nitroso end-groups. The resultant materials exhibited good thermal stability and mesoporous nature. The highest BET surface area of 48.1 $m^2\ g^{-1}$ was observed for the azodioxy oligomer of 2,4,6-tris(4-nitrosophenyl)pyridine. The CO_2 uptakes of *E*-azodioxy oligomers and polymers were roughly comparable, with the highest value of 6.2 mg g^{-1} observed for the amine-based azodioxy oligomer. A comparison of the experimental and simulated PXRD patterns of the DFT calculated geometries strongly suggested that serrated AA' layers may be preferred over perfectly eclipsed AA layers when/if 2D layers are organized into periodic polymer networks, especially in case of the azodioxy-linked triphenyltriazine-based building units.

Overall, the results of the current study, in particular novel synthetic insights, could be used for the design of new functional azodioxy-linked porous materials derived from polynitroso building blocks of predefined geometry.

Funding statement

This work has been fully supported by Croatian Science Foundation under the project IP-2020-02-4467.

Data availability statement

Data included in article/supplementary material/referenced in article.

Additional information

Supplementary content related to this article has been published online at.

CRediT authorship contribution statement

Nikola Cindro: Investigation, Methodology, Writing – original draft. **Željka Car:** Investigation, Methodology, Writing – original draft. **Vesna Petrović Peroković:** Investigation, Methodology, Writing – original draft. **Mladen Borovina:** Investigation, Methodology, Visualization, Writing – original draft. **Barbara Panić:** Investigation, Visualization, Writing – original draft. **Ivan Kodrin:** Conceptualization, Investigation, Methodology, Project administration, Software, Supervision, Validation, Visualization, Writing – original draft, Writing – review & editing. **Ivana Biljan:** Conceptualization, Funding acquisition, Investigation, Methodology, Supervision, Validation, Visualization, Writing – original draft, Writing – review & editing.

Declaration of competing interest

The authors declare the following financial interests/personal relationships which may be considered as potential competing interests:Ivana Biljan reports financial support was provided by Croatian Science Foundation. The authors declare the following conflict of interest: I. Kodrin is an Associate Editor of Heliyon (section: Chemistry).

Acknowledgment

The support of project CIuK (Grant KK.01.1.1.02.0016) co-financed by the Croatian Government and the European Union through the European Regional Development Fund - Competitiveness and Cohesion Operational Program are acknowledged. The authors acknowledge the CERIC-ERIC Consortium for the access to experimental facilities.

Appendix A. Supplementary data

Supplementary data to this article can be found online at https://doi.org/10.1016/j.heliyon.2023.e21781.

References

[1] D. Beaudoin, J.D. Wuest, Dimerization of aromatic C-nitroso compounds, Chem. Rev. 116 (2016) 258–286.
[2] D. Beaudoin, T. Maris, J.D. Wuest, Constructing monocrystalline covalent organic networks by polymerization, Nat. Chem. 5 (2013) 830–834.
[3] H. Vančik, Aromatic C-Nitroso Compounds, Springer Verlag, New York, 2013.
[4] G. Gallo, A. Mihanović, I. Rončević, R. Dinnebier, H. Vančik, Crystal structure and ON-OFF polymerization mechanism of poly(1,4-phenyleneazine-*N,N*-dioxide), a possible wide bandgap semiconductor, Polymer 214 (2021), 123235.
[5] L. Matasović, B. Panić, M. Bubaš, H. Vančik, I. Biljan, I. Rončević, Modulating electronic properties of dinitrosoarene polymers, J. Mater. Chem. C 10 (2022) 5433–5446.
[6] N.P. Hacker, Investigation of the polymerization of 1,4-dinitrosobenzene by low-temperature infrared and UV absorption spectroscopy, Macromolecules 26 (1993) 5937–5942.
[7] B.G. Gowenlock, G.B. Richter-Addo, Dinitroso and polynitroso compounds, Chem. Soc. Rev. 34 (2005) 797–809.
[8] P. Bibulić, I. Rončević, M. Špadina, I. Biljan, H. Vančik, Isothermal and isoconversional modeling of solid-state nitroso polymerization, J. Phys. Chem. A 124 (2020) 10726–10735.
[9] I. Rončević, P. Bibulić, H. Vančik, I. Biljan, Solution equilibria of aromatic dinitroso compounds: a combined NMR and DFT study, Struct. Chem. 29 (2018) 1489–1497.
[10] H. Vančik, V. Šimunić-Mežnarić, E. Meštrović, S. Milovac, K. Majerski, J. Veljković, Solid state photochromism and thermochromism in nitroso monomer-dimer equilibrium, J. Phys. Chem. B 106 (2002) 1576–1580.
[11] A. Knežević, T. Medančić, S. Milovac, I. Biljan, I. Halasz, H. Vančik, Photothermal reactions of nitrosobenzene and halonitrosobenzenes in solid-state, Croat. Chem. Acta 84 (2011) 21–24.
[12] I. Halasz, E. Meštrović, H. Čičak, Z. Mihalić, H. Vančik, Solid-state reaction mechanisms in monomer-dimer interconversions of *p*-bromonitrosobenzene. Single-crystal-to-single-crystal photodissociation and formation of new non-van der Waals close contacts, J. Org. Chem. 70 (2005) 8461–8467.
[13] K. Varga, J. Volarić, H. Vančik, Crystal disordering and organic solid-state reactions, CrystEngComm 17 (2015) 1434–1438.
[14] P. Bibulić, I. Rončević, K. Varga, Z. Mihalić, H. Vančik, Structure and topochemistry of azodioxide oligomers in solid state, J. Mol. Struct. 1104 (2016) 85–90.
[15] P. Bibulić, I. Rončević, V. Bermanec, H. Vančik, Polymerization of 1,4-dinitrosobenzene: kinetics and submicrocrystal structure, Croat. Chem. Acta 90 (2017) 383–389.
[16] I. Biljan, H. Vančik, Aromatic C-nitroso compounds and their dimers: a model for probing the reaction mechanisms in crystalline molecular solids, Crystals 7 (2017) 376.
[17] K. Varga, N. Lešić, B. Bogović, M. Pisačić, B. Panić, I. Biljan, I. Novak, H. Vančik, Thermally-induced reactions of aromatic crystalline nitroso compounds, ChemistrySelect 4 (2019) 4709–4717.
[18] S. Das, P. Heasman, T. Ben, S. Qiu, Porous organic materials: strategic design and structure-function correlation, Chem. Rev. 117 (2017) 1515–1563.
[19] M.G. Mohamed, A.F.M. EL-Mahdy, M.G. Kotp, S.-W. Kuo, Advances in porous organic polymers: syntheses, structures, and diverse applications, Mater, Adv 3 (2022) 707–733.
[20] H.A. Patel, J. Byun, C.T. Yavuz, Carbon dioxide capture adsorbents: Chemistry and methods, ChemSusChem 10 (2017) 1303–1317.
[21] O. Hoegh-Guldberg, P.J. Mumby, A.J. Hooten, R.S. Steneck, P. Greenfield, E. Gomez, C.D. Harvell, P.F. Sale, A.J. Edwards, K. Caldeira, N. Knowlton, C.M. Eakin, R. Iglesias-Prieto, N. Muthiga, R.H. Bradbury, A. Dubi, M.E. Hatziolos, Coral reefs under rapid climate change and ocean acidification, Science 318 (2007) 1737–1742.
[22] W. Wang, M. Zhou, D. Yuan, Carbon dioxide capture in amorphous porous organic polymers, J. Mater. Chem. A 5 (2017) 1334–1347.
[23] P. Bhanja, A. Modak, A. Bhaumik, Porous organic polymers for CO_2 storage and conversion reactions, ChemCatChem 11 (2019) 244–257.
[24] L. Shao, Y. Li, J. Huang, Y.-N. Liu, Synthesis of triazine-based porous organic polymers derived N-enriched porous carbons for CO_2 capture, Ind. Eng. Chem. Res. 57 (2018) 2856–2865.
[25] K.S. Song, P.W. Fritz, A. Coskun, Porous organic polymers for CO_2 capture, separation and conversion, Chem. Soc. Rev. 51 (2022) 9831–9852.
[26] H. Gao, Q. Li, S. Ren, Recent advances on CO_2 capture by porous organic polymers, Curr. Opin. Green Sustainable Chem. 16 (2018) 33–38.
[27] G. Singh, J. Lee, A. Karakoti, R. Bahadur, J. Yi, D. Zhao, K. Albahily, A. Vinu, Emerging trends in porous materials for CO_2 capture and conversion, Chem. Soc. Rev. 49 (2020) 4360–4404.
[28] M. Ejaz, M.G. Mohamed, S.-W. Kuo, Solid state chemical transformation provides a fully benzoxazine-linked porous organic polymer displaying enhanced CO_2 capture and supercapacitor performance, Polym. Chem. 14 (2023) 2494–2509.
[29] A.O. Mousa, C.-H. Chuang, S.-W. Kuo, M.G. Mohamed, Strategic design and synthesis of ferrocene linked porous organic frameworks toward tunable CO_2 capture and energy storage, Int. J. Mol. Sci. 24 (2023), 12371.
[30] A.O. Mousa, M.G. Mohamed, C.-H. Chuang, S.-W. Kuo, Carbonized aminal-linked porous organic polymers containing pyrene and triazine units for gas uptake and energy storage, Polymers 15 (2023) 1891.
[31] M.G. Mohamed, S.-Y. Chang, M. Ejaz, M.M. Samy, A.O. Mousa, S.-W. Kuo, Design and synthesis of bisulfone-linked two-dimensional conjugated microporous polymers for CO_2 adsorption and energy storage, Molecules 28 (2023) 3234.
[32] M.G. Mohamed, W.-C. Chang, S.-W. Kuo, Crown ether- and benzoxazine-linked porous organic polymers displaying enhanced metal ion and CO_2 capture through solid-state chemical transformation, Macromolecules 55 (2022) 7879–7892.
[33] C. Kim, S.N. Talapaneni, L. Dai, Porous carbon materials for CO_2 capture, storage and electrochemical conversion, Materials Reports: Energy 3 (2023), 100199.
[34] M.G. Mohamed, M.M. Samy, T.H. Mansoure, C.-J. Li, W.-C. Li, J.-H. Chen, K. Zhang, S.-W. Kuo, Microporous carbon and carbon/metal composite materials derived from bio-benzoxazine-linked precursor for CO_2 capture and energy storage applications, Int. J. Mol. Sci. 23 (2022) 347.
[35] Y. Zhu, H. Long, W. Zhang, Imine-linked porous polymer frameworks with high small gas (H_2, CO_2, CH_4, C_2H_2) uptake and CO_2/N_2 selectivity, Chem. Mater. 25 (2013) 1630–1635.
[36] G. Gu, D. Liu, W. Huang, J. Liu, R. Yang, Synthesis of covalent triazine-based frameworks with high CO_2 adsorption and selectivity, Polym. Chem. 6 (2015) 7410–7417.
[37] X. Zhu, S.M. Mahurin, S.-H. An, C.-L. Do-Thanh, C. Tian, Y. Li, L.W. Gill, E.W. Hagaman, Z. Bian, J.-H. Zhou, J. Hu, H. Liu, S. Dai, Efficient CO_2 capture by a task-specific porous organic polymer bifunctionalized with carbazole and triazine groups, Chem. Commun. 50 (2014) 7933–7936.
[38] S. Nandi, U. Werner-Zwanzigerb, R. Vaidhyanathan, A triazine-resorcinol based porous polymer with polar pores and exceptional surface hydrophobicity showing CO_2 uptake under humid conditions, J. Mater. Chem. A 3 (2015) 21116–21122.
[39] S. Gu, J. Guo, Q. Huang, J. He, Y. Fu, G. Kuang, C. Pan, G. Yu, 1,3,5-Triazine-Based microporous polymers with tunable porosities for CO_2 capture and fluorescent sensing, Macromolecules 50 (2017) 8512–8520.
[40] S. Kumar, A. Hassan, N. Das, J. Koh, Triazine based nanoarchitectonics of porous organic polymers for CO_2 storage, Mater. Lett. 313 (2022), 131757.
[41] M.G. Rabbani, H.M. El-Kaderi, Synthesis and characterization of porous benzimidazole-linked polymers and their performance in small gas storage and selective uptake, Chem. Mater. 24 (2012) 1511–1517.
[42] H.A. Patel, S.H. Je, J. Park, Y. Jung, A. Coskun, C.T. Yavuz, Directing the structural features of N_2-phobic nanoporous covalent organic polymers for CO_2 capture and separation, Chem. Eur J. 20 (2014) 772–780.
[43] H.A. Patel, S.H. Je, J. Park, D.P. Chen, Y. Jung, C.T. Yavuz, A. Coskun, Unprecedented high-temperature CO_2 selectivity in N_2-phobic nanoporous covalent organic polymers, Nat. Commun. 4 (2013) 1357.
[44] P. Arab, M.G. Rabbani, A.K. Sekizkardes, T. İslamoğlu, H.M. El-Kaderi, Copper(I)-Catalyzed synthesis of nanoporous azo-linked polymers: impact of textural properties on gas storage and selective carbon dioxide capture, Chem. Mater. 26 (2014) 1385–1392.
[45] P. Arab, E. Parrish, T. İslamoğlu, H.M. El-Kaderi, Synthesis and evaluation of porous azo-linked polymers for carbon dioxide capture and separation, J. Mater. Chem. A 3 (2015) 20586–20594.

[46] R. Bera, M. Ansari, A. Alam, N. Das, Triptycene, phenolic-OH, and azo-functionalized porous organic polymers: efficient and selective CO_2 capture, ACS Appl. Polym. Mater. 1 (2019) 959–968.

[47] M.M. Abdelnaby, T.A. Saleh, M. Zeama, M.A. Abdalla, H.M. Ahmed, M.A. Habib, Azo-linked porous organic polymers for selective carbon dioxide capture and metal ion removal, ACS Omega 7 (2022) 14535–14543.

[48] L. Tao, F. Niu, D. Zhang, J. Liu, T. Wang, Q. Wang, Azo-bridged covalent porphyrinic polymers (Azo-CPPs): synthesis and CO_2 capture properties, RSC Adv. 5 (2015) 96871–96878.

[49] B. Nath, W.H. Li, J.H. Huang, G.E. Wang, Z.H. Fu, M.S. Yao, G. Xu, A new azodioxy-linked porphyrin-based semiconductive covalent organic framework with I_2 doping-enhanced photoconductivity, CrystEngComm 18 (2016) 4259–4263.

[50] B. Panić, T. Frey, M. Borovina, K. Konopka, M. Sambolec, I. Kodrin, I. Biljan, Synthesis and characterization of benzene- and triazine-based azo-bridged porous organic polymers, Polymers 15 (2023) 229.

[51] T. Frey, B. Panić, P. Šutalo, M. Borovina, I. Biljan, I. Kodrin, Prediction of CO_2 adsorption properties of azo, azoxy and azodioxy-linked porous organic polymers guided by electrostatic potential, CrystEngComm 25 (2023) 3870.

[52] P. Šutalo, M. Pisačić, I. Biljan, I. Kodrin, Benzene and triazine-based porous organic polymers with azo, azoxy and azodioxy linkages: a computational study, CrystEngComm 24 (2022) 4748–4763.

[53] D.O. Ojwang, J. Grins, G. Svensson, The adsorption kinetics of CO_2 on copper hexacyanoferrate studied by thermogravimetric analysis, Microporous Mesoporous Mater. 272 (2018) 70–78.

[54] R. Dovesi, A. Erba, R. Orlando, C.M. Zicovich-Wilson, B. Civalleri, L. Maschio, M. Rérat, S. Casassa, J. Baima, S. Salustro, B. Kirtman, Quantum-mechanical condensed matter simulations with CRYSTAL, WIREs Comput. Mol. Sci. 8 (2018) e1360.

[55] J.P. Perdew, J.A. Chevary, S.H. Vosko, K.A. Jackson, M.R. Pederson, D.J. Singh, C. Fiolhais, Atoms, molecules, solids, and surfaces: applications of the generalized gradient approximation for exchange and correlation, Phys. Rev. B 46 (1992) 6671–6687.

[56] S. Grimme, J. Antony, S. Ehrlich, H. Krieg, A consistent and accurate ab initio parametrization of density functional dispersion correction (DFT-D) for the 94 elements H-Pu, J. Chem. Phys. 132 (2010), 154104.

[57] D. Vilela Oliveira, J. Laun, M.F. Peintinger, T. Bredow, BSSE-correction scheme for consistent Gaussian basis sets of double- and triple-zeta valence with polarization quality for solid-state calculations, J. Comput. Chem. 40 (2019) 2364–2376.

[58] T. Björkman, CIF2Cell: generating geometries for electronic structure programs, Comput. Phys. Commun. 182 (2011) 1183–1186.

[59] K. Momma, F. Izumi, VESTA 3 for three-dimensional visualization of crystal, volumetric and morphology data, J. Appl. Crystallogr. 44 (2011) 1272–1276.

[60] C.F. Macrae, I. Sovago, S.J. Cottrell, P.T.A. Galek, P. McCabe, E. Pidcock, M. Platings, G.P. Shields, J.S. Stevens, M. Towler, P.A. Wood, Mercury 4.0: from visualization to analysis, design and prediction, J. Appl. Crystallogr. 53 (2020) 226–235.

[61] B.G. Gowenlock, G.B. Richter-Addo, Preparations of C-nitroso compounds, Chem. Rev. 104 (2004) 3315–3340.

[62] L. Anderson, M. Cameron, B.G. Gowenlock, J. McEwen, Properties and spectroscopic studies of polymeric dinitrosobenzenes, J. Chem. Soc. Perkin Trans. 2 (1992) 243–245.

[63] I. Halasz, I. Biljan, P. Novak, E. Meštrović, J. Plavec, G. Mali, V. Smrečki, H. Vančik, Cross-dimerization of nitrosobenzenes in solution and in solid state, J. Mol. Struct. 918 (2009) 19–25.

[64] I. Biljan, G. Cvjetojević, V. Smrečki, P. Novak, G. Mali, J. Plavec, D. Babić, Z. Mihalić, H. Vančik, Nitrosobenzene cross-dimerization: structural selectivity in solution and in solid state, J. Mol. Struct. 979 (2010) 22–26.

[65] W. Chen, W. Yan, S. Wu, Z. Xu, K.W.K. Yeung, C. Yi, Preparation and properties of novel triphenylpyridine-containing hyperbranched polyimides derived from 2,4,6-tris(4- aminophenyl)pyridine under microwave irradiation, Macromol. Chem. Phys. 211 (2010) 1803–1813.

[66] A. Halder, S. Kandambeth, B.P. Biswal, G. Kaur, N.C. Roy, M. Addicoat, J.K. Salunke, S. Banerjee, K. Vanka, T. Heine, S. Verma, R. Banerjee, Decoding the morphological diversity in two dimensional crystalline porous polymers by core planarity modulation, Angew. Chem. Int. Ed. 55 (2016) 7806–7810.

[67] R. Gomes, P. Bhanjaa, A. Bhaumik, A triazine-based covalent organic polymer for efficient CO_2 adsorption, Chem. Commun. 51 (2015) 10050–10053.

[68] A. Jiménez-Almarza, A. López-Magano, R. Mas-Ballesté, J. Alemán, Tuning the activity-stability balance of photocatalytic organic materials for oxidative coupling reactions, ACS Appl. Mater. Interfaces 14 (2022) 16258–16268.

[69] R. Purushothaman, H.S. Vaitinadin, Inclusion of covalent triazine framework into fluorinated polyimides to obtain composites with low dielectric constant, J. Appl. Polym. Sci. 137 (2020), e49083.

[70] P. Puthiaraj, Y.-R. Lee, S. Zhang, W.-S. Ahn, Triazine-based covalent organic polymers: design, synthesis and applications in heterogeneous catalysis, J. Mater. Chem. A 4 (2016) 16288–16311.

[71] A.F.M. El-Mahdy, C.H. Kuo, A. Alshehri, C. Young, Y. Yamauchi, J. Kim, S.W. Kuo, Strategic design of triphenylamine- and triphenyltriazine-based two-dimensional covalent organic frameworks for CO_2 uptake and energy storage, J. Mater. Chem. A 6 (2018) 19532–19541.

[72] L. Zhai, N. Huang, H. Xu, Q. Chen, D. Jiang, A backbone design principle for covalent organic frameworks: the impact of weakly interacting units on CO_2 adsorption, Chem. Commun. 53 (2017) 4242–4245.

[73] Y. Peng, Y. Huang, Y. Zhu, B. Chen, L. Wang, Z. Lai, Z. Zhang, M. Zhao, C. Tan, N. Yang, F. Shao, Y. Han, H. Zhang, Ultrathin two-dimensional covalent organic framework nanosheets: preparation and application in highly sensitive and selective DNA detection, J. Am. Chem. Soc. 139 (2017) 8698–8704.

[74] B.T. Koo, W.R. Dichtel, P. Clancy, A classification scheme for the stacking of two-dimensional boronate ester-linked covalent organic frameworks, J. Mater. Chem. 22 (2012) 17460–17469.

[75] E.L. Spitler, B.T. Koo, J.L. Novotney, J.W. Colson, F.J. Uribe-Romo, G.D. Gutierrez, P. Clancy, W.R. Dichtel, A 2D covalent organic framework with 4.7-nm pores and insight into its interlayer stacking, J. Am. Chem. Soc. 133 (2011) 19416–19421.

[76] A.M. Pütz, M.W. Terban, S. Bette, F. Haase, R.E. Dinnebier, B.V. Lotsch, Total scattering reveals the hidden stacking disorder in a 2D covalent organic framework, Chem. Sci. 11 (2020) 12647–12654.

[77] R. Dawson, E. Stöckel, J.R. Holst, D.J. Adams, A.I. Cooper, Microporous organic polymers for carbon dioxide capture, Energy Environ. Sci. 4 (2011) 4239–4245.